Insights into the role of magnetoelastic anisotropy in the magnetization reorientation of magnetic nanowires

D. C. Leitao,[1,*] J. Ventura,[1] C. T. Sousa,[1] A. M. Pereira,[1] J. B. Sousa,[1] M. Vazquez,[2] and J. P. Araujo[1]

[1]*IFIMUP and IN—Institute of Nanoscience and Nanotechnology, Department of Physics and Astronomy, Faculdade de Ciencias da Universidade do Porto, Rua do Campo Alegre 678, P-4169-007 Porto, Portugal*

[2]*Instituto de Ciencia de Materiales de Madrid, CSIC Campus Cantoblanco, E-28049 Madrid, Spain*

(Received 11 March 2011; published 21 July 2011)

Understanding the physical properties of magnetic nanowires (NWs) is of crucial importance due to their potential technological applications. In this paper we report a detailed study on the temperature dependence of the magnetic [$M(T)$] and magnetotransport [MR(T)] properties of Ni and NiFe NWs grown on anodic aluminum oxide templates. While the behavior of the NiFe NWs reflected the presence of a strong shape anisotropy, Ni NWs showed anomalous $M(T)$ and MR(T). The deviations from the expected $M(T)$ and MR(T) behaviors suggest a reorientation of the magnetization easy axis with decreasing temperature. We then extracted the temperature variation of the angle between the magnetization and the NW longitudinal axis, and found an increase from 0° at 370 K to ∼43° at 5 K. Using a fourth-order magnetic anisotropy energy model we were able to successfully explain our results and show that the presence of a magnetoelastic anisotropy contribution due to the compressive stress acting in the NWs is the main origin of the observed magnetization reorientation.

DOI: 10.1103/PhysRevB.84.014410 PACS number(s): 75.30.Gw, 73.63.−b, 75.75.−c, 81.07.Gf

I. INTRODUCTION

Unique and interesting phenomena are expected both from fundamental and technological points of view as the geometrical dimensions of magnetic materials become comparable to the electron mean free path or the domain-wall width. In particular, systems composed of magnetic nanowires (NWs) with reduced dimensions (few nanometers) can exhibit considerable changes in their physical properties, including quasi-ideal magnetization (M) reversal,[1] quantized spin transport,[2] or electron localization effects.[3]

Due to high aspect ratios, one expects magnetic NWs to exhibit a behavior dominated by strong shape anisotropy and hence a magnetization easy axis lying along the longitudinal direction. However, when packed in a dense array, a pronounced interplay between the different components of the total magnetic anisotropy appears, which can lead to changes in the orientation of the magnetic easy axis and even to a crossover from the parallel to the perpendicular direction, relative to the NW long axis.[4,5] By changing the geometrical dimensions (diameter and length)[4,6] or the composition[7,8] of the NWs, one can effectively tune the corresponding magnetic easy-axis orientation.

Arrays of Ni NWs stand as a particular case exhibiting an anomalous magnetic behavior with decreasing temperature (T). Some authors attributed the observed decrease in coercivity and remanence with decreasing T to the irregular surface morphologies of the NWs,[9] while others suggested the presence of a competition between shape and magnetoelastic anisotropies in samples grown using either polycarbonate membranes[10,11] or anodic aluminum oxide (AAO) templates.[12,13]

Interestingly, a similar behavior was reported for ultrathin Ni films where a spin-reorientation transition (SRT) from in plane to out of plane appeared with decreasing thickness.[14] In this case, the deposition of few monolayers of magnetic material induced drastic changes in the magnetic easy axis, due to the presence of a strong perpendicular surface anisotropy and enhanced stress.[14–16]

Besides magnetization measurements, electrical and magnetotransport experiments can also give different insights into magnetic processes in nanostructures. However, and even though the magnetism of ferromagnetic NWs consisting of an interacting dense array or of a single, isolated wire has been exhaustively studied,[6,8,12,13,17,18] to the best of our knowledge, few reports can be found on the T dependence of both electrical resistance [$R(T)$][19,20] and magnetoresistance [MR(T)].[21,22] Kamalakar *et al.*[20] studied the $R(T)$ behavior of isolated and matrix embedded Ni NWs. They observed a reduced Debye temperature in comparison to bulk Ni and a suppression of the magnetic contribution to $R(T)$ with decreasing NW diameter.[20] This behavior was attributed to the damping of the lattice vibration modes due to the confined dimensionality. In addition, magnetotransport measurements (10–300 K) performed in single strands of Ni and NiFe NWs emphasized mainly the identification of magnetization reversal modes.[21,22] Nevertheless, and contrary to what was observed previously using magnetic measurements,[12,13] these transport studies did not report any M reorientation for AAO-embedded Ni NWs.

In this paper we report magnetic and magnetotransport measurements performed in arrays of NiFe and Ni NWs embedded in AAO membranes and grown by pulsed electrodeposition. NiFe NWs showed typical $M(T)$ and MR(T) behaviors, translating the presence of well-defined shape anisotropy. On the other hand, for Ni NWs we obtained a monotonic change of the angle between the magnetization and the NWs' longitudinal axis with decreasing temperature. Such behavior is observed independently by $M(T)$ and MR(T) measurements. A fourth-order magnetic anisotropy energy model was used to successfully explain our results, showing that the magnetoelastic anisotropy component is the main source for the observed spin reorientation transition.

II. EXPERIMENTAL DETAILS

For the growth of magnetic NWs we used AAO templates obtained by a standard two-step anodization method of high-purity (99.997%) Al foils.[23] After an electropolishing pre-treatment, the Al foils were anodized in a 0.3*M* oxalic acid solution at ∼4 °C and under an applied potential of 40 V.[24] The first anodization was carried out for 24 h while the second lasted 1 h. These anodization conditions resulted in nanopores with an average diameter of ∼35 nm, separation of ∼105 nm, and ∼2.5 μm in length.

At the bottom of each nanopore, a non-conductive alumina barrier layer is present, with a nominal thickness that depends on the applied anodization potential.[25] For the conditions used we estimate a barrier layer of ∼50 nm. However, for the filling of the nanopores by electrodeposition, such an insulator layer must be removed or thinned down. Therefore, we reduced the barrier layer to a nominal thickness of ∼3 nm, originating dendrites in the process (small channels in the alumina layer).[26]

The procedure employed retains both the characteristic AAO geometrical features and the underlying Al substrate. Moreover, the barrier-layer thickness is expected to vary slightly from pore to pore, leading to different barrier-layer resistance for each nanopore and consequently to distinctive local deposition rates. A detailed study on the influence of the barrier-layer thickness on the nanopore filling uniformity will be presented elsewhere.[27]

A pulsed electrodeposition method was then used to grow the metallic NWs inside the AAO.[26] First, the dendrite channels were filled with Cu from a solution composed of $CuSO_4 \cdot 5H_2O$ and H_3BO_3 [Fig. 1(a)]. The electrodeposition was performed at ∼303 K with an applied current density of 26 mA/cm^2. The main cylindrical nanopore was subsequently filled with magnetic materials (Ni or NiFe). A compositional ratio was estimated for NiFe alloy NWs to be 80:20 from energy dispersive spectroscopy (EDS) analysis, as expected from the recipe.[28] Further details regarding the corresponding electrodeposition conditions can be found elsewhere.[8]

The surface of the samples was then ion milled, setting the final dimensions of the NWs reaching the surface to 2 μm. Figure 1(b) shows a top-view image of the AAO surface with only a few NWs reaching the top (bright spots). A NW density of ∼4×10^7 NWs/cm^2 is estimated (compare to the AAO template density of ∼10^9 pores/cm^2). Such a small filling ratio (∼0.1%) is a consequence of the nonuniformity of the alumina barrier thickness and also of the local detachment of the AAO from the underlying Al. Nevertheless, this low NW density allows us to study here the transport properties of a small number of magnetic NWs. The studied samples are thus composed by three distinct segments: the (metallic) magnetic NWs ramify into Cu metallic dendritic channels, which then finish at a ∼3 nm alumina barrier layer. The bottom and top electrodes are then the underneath Al foil and a sputter-deposited Au thin film, respectively.

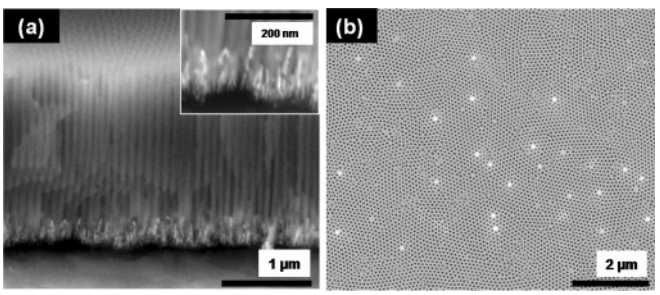

FIG. 1. SEM images of a Cu/NiFe sample: (a) AAO cross-section images with dendrites filled with Cu and (b) top image of Cu/NiFe NWs. Notice that only a small number (0.1%) of channels is filled.

The morphology and structure of the samples were studied by scanning electron microscopy (SEM) with a low-vacuum FEI Quanta 400FEG and by x-ray diffraction (XRD), using a X'Pert PRO diffractometer in the θ-2θ geometry (Cu $K\alpha$ line, $\lambda = 1.5406$ Å). $M(T)$ characterization was performed with a Quantum Design superconducting quantum interference device (SQUID), and the $R(T)$ and MR(T) measurements were performed with a pseudo-four-probe dc method from 20 to 300 K and applied magnetic fields up to 6.5 kOe.

III. EXPERIMENTAL RESULTS

A. Structural characterization

Figure 2 shows XRD scans for the studied samples. To attain improved details regarding the NW diffraction patterns, the Al substrate was previously removed. Two main diffraction peaks were observed for both Ni and NiFe NWs, corresponding to the fcc (111) and (220) structure. A preferential fcc structure strongly textured along ⟨110⟩ is present, as typical for template-assisted electrodeposited NWs with high aspect ratios.[10,17,29] Using the Scherrer equation and the (220) peak, we estimate a grain size (GS) of 100 and 30 nm for Ni and NiFe NWs, respectively. Notice that a GS ∼ 5–20 nm was reported for Ni NWs electrodeposited using a higher current density

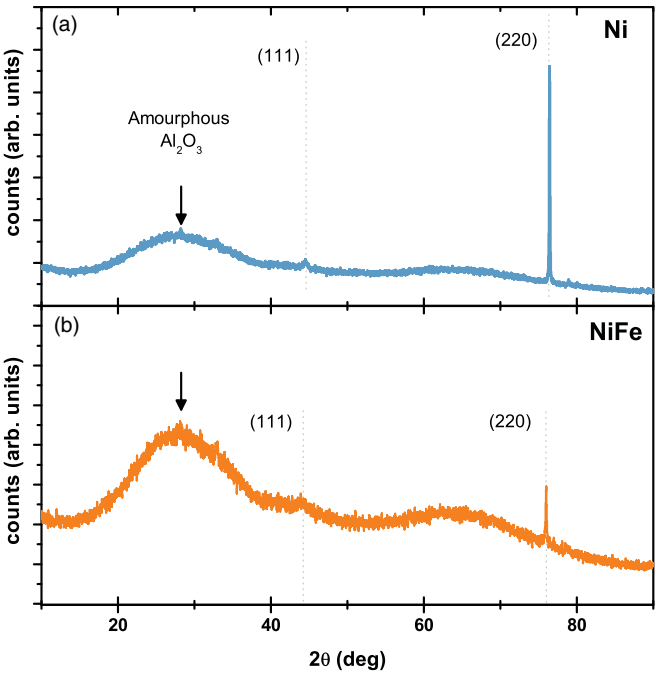

FIG. 2. (Color online) θ-2θ XRD scans of (a) Ni, (b) NiFe, compared to the corresponding powder diffraction peaks obtained from Ref. 52.

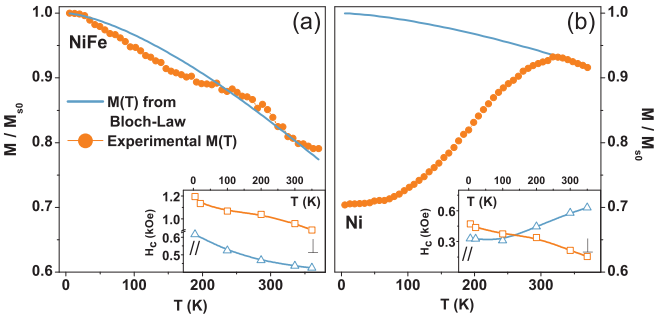

FIG. 3. (Color online) Longitudinal $M(T)$ curves of (a) NiFe and (b) Ni NWs. The solid lines represent the expected behavior of $M(T)$ according to Eq. (1). The inset shows $H_c(T)$ for Ni NWs in both configurations; the lines are guides to the eye.

than the one reported here.[6] The wide bump visible at $\sim 30^\circ$ corresponds to the amorphous alumina from the AAO.

B. Magnetic properties

Figure 3 shows the field-cooled magnetization versus temperature curves of the NW samples, measured parallel to their longitudinal direction with an applied magnetic field of 50 Oe. For NiFe, one observes the expected growth of the magnetization with decreasing temperature characteristic of a well-defined uniaxial anisotropy material [Fig. 3(a)]. In the spin-wave regime ($T \ll T_C$), one has

$$M_s(T) = M_s^0 \left[1 - \beta \left(\frac{T}{T_C} \right)^{3/2} \right], \qquad (1)$$

where T_C is the Curie temperature, M_s^0 is the spontaneous magnetization at 0 K [$M_s^0(\mathrm{Ni}) = 510$ emu/cm^3 and $M_s^0(\mathrm{NiFe}) = 880$ emu/cm^3], and the constant β is a fitting parameter.[30] The solid line in Fig. 3(a) displays the theoretical $M(T)$ calculated from Eq. (1), with $T_C^{\mathrm{bulk}}(\mathrm{NiFe}) = 850$ K and $\beta = 0.41$. The latter was determined from the Arrot plot representation of $M(H)$ curves measured at different temperatures (not shown). Moreover, taking $T_C^{\mathrm{NW}} \simeq T_C^{\mathrm{bulk}}$ is considered a fair approach, since a significative decrease of T_C in strongly confined systems was reported only for NWs with diameters smaller than 10 nm.[31,32]

On the other hand, the Ni sample displays an anomalous $M(T)$ behavior when compared with NiFe and theoretical expectations [Fig. 3(b)]. In fact, the solid line shows the $M(T)$ calculated using Eq. (1), with $T_C^{\mathrm{bulk}}(\mathrm{Ni}) = 630$ K and $\beta = 0.18$ (also determined from Arrot plot analyses; not shown). These values are in accordance with previously reported ones.[32] The experimental $M(T)$ data exhibits a slight increase with decreasing temperature [following closely Eq. (1)] down to ~ 330 K. This trend is then followed by a continuous decrease of $M(T)$ down to $\sim 0.7 M_s^0$ at 5 K. Such a deviation from the expected $M(T)$ behavior indicates that M is moving away from the NW longitudinal axis, pointing toward a reorientation of the magnetization as T decreases,[32,33] as will be discussed below.

Interestingly, such behavior is also in accordance with the failure of the thermal activation model in explaining the observed anomalous coercive field [H_c(T)] trend in Ni NWs [see the inset of Fig. 3(b) for transverse and parallel applied magnetic field].[8] While NiFe shows a continuous increase of $H_c(T)$ with decreasing temperature [see the inset of Fig. 3(a)] characteristic of the dominant shape anisotropy (K_{sh}), the observed $H_c(T)$ for Ni points toward the presence of a weakly defined easy axis.

C. Magnetotransport properties

The temperature-dependent MR of the NWs was also studied in detail. First, notice that metallic-like $R(T)$ curves were obtained in both samples, leading us to conclude that the thin alumina barrier between the dendrites and the Al foil does not affect considerably our transport measurements [see the inset of Fig. 4(d)].[34] Such a barrier may even be absent, so that the dendritic channels directly contact the Al electrode; in other cases they may be so thin that the resulting resistance is low.

In this work we defined the transverse and parallel MR ($\mathrm{MR}^{\perp,\parallel}$) as

$$\mathrm{MR}^{\perp,\parallel} = \frac{R^{\perp,\parallel}(H) - R^{\perp,\parallel}(H_{\max})}{R^{\perp,\parallel}(H_{\max})}, \qquad (2)$$

where $R^{\perp}$ ($R^{\parallel}$) is the resistance measured transverse (parallel) to the electrical current (or equivalently, to the long axis of the NWs), and $H_{\max}$ is the maximum applied magnetic field.

Figure 4 displays MR curves for NiFe and Ni NWs at 300 and 20 K.[35] The bell-shaped $\mathrm{MR}^{\perp}$ curves display values consistent with those reported in the literature (1%–1.8% for Ni and 1.2%–2.4% for NiFe NWs).[21,22] For NiFe NWs we observe the characteristic anisotropic magnetoresistance (AMR) behavior in the considered magnetic field and temperature ranges, with positive $\mathrm{MR}^{\perp}$ denoting M reversal mainly through rotation processes in the transverse geometry, and negligible $\mathrm{MR}^{\parallel}_{\mathrm{NiFe}}$ values, due to magnetization reversal by

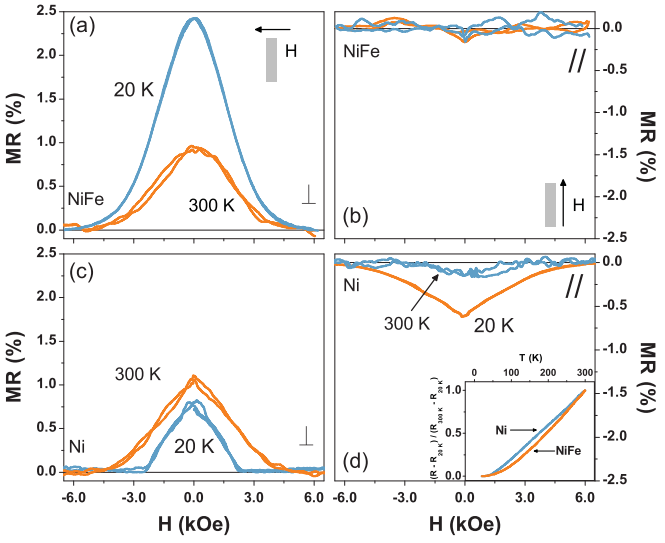

FIG. 4. (Color online) Magnetoresistance curves at 300 and 20 K: (a) $\mathrm{MR}^{\perp}$ and (b) $\mathrm{MR}^{\parallel}$ for NiFe NWs; (c) $\mathrm{MR}^{\perp}$ and (d) $\mathrm{MR}^{\parallel}$ for Ni NWs. The inset shows normalized $R(T)$ curves of the NiFe and Ni samples, displaying a metallic-like behavior ($dR/dT > 0$).

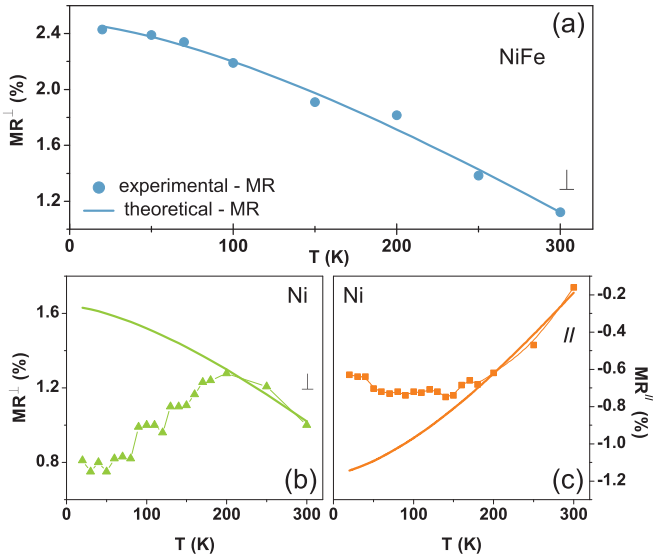

FIG. 5. (Color online) Temperature dependence of (a) $MR^{\perp}$ for NiFe, (b) $MR^{\perp}$, and (c) $MR^{\parallel}$ for Ni. The lines are the best fits of Eq. (3) to the experimental data.

domain-wall propagation for H along the longitudinal axis [Fig. 4(b)].

For Ni NWs we also observe the expected $MR^{\perp}$ shape. However, an immediate difference is visible on the parallel configuration for which a triangular $MR^{\parallel}_{Ni}$ curve is observed, together with clearly higher MR values [$\sim$0.8% at 20 K; Fig. 4(d)]. This again suggests a magnetic behavior no longer dominated solely by shape anisotropy for Ni NWs.

Figure 5 shows the MR(T) curves for both NW samples. NiFe shows an increase in the MR values with decreasing temperature, resulting from the increase of the spontaneous magnetization and reduction of thermal scattering [Fig. 5(a)]. This MR(T) behavior is characteristic of materials with a well-defined uniaxial anisotropy, i.e., a strong M easy axis. In our case of high-aspect-ratio particles, the presence of a dominant K_{sh} [$K_{sh} = \pi M_s^2(T)$] is expected and was corroborated previously by temperature-dependent H_c measurements.[8] On the other hand, Ni NWs initially display an increase in the MR magnitude with decreasing temperature [Figs. 5(b) and 5(c)], readily followed by a MR decrease.

It is known that M reversal in NWs takes place mainly by (localized) spin rotation.[1,8,18] One can therefore, in a simple approximation, consider[36]

$$\mathrm{MR}(T) \propto \cos^2[\theta(H,T)] \propto \left[\frac{M_s(T)}{M_s^0}\right]^2, \qquad (3)$$

where θ is the angle between M and the current, which flows along the NW longitudinal direction. The line in Fig. 5(a) shows the fit of the $MR_{NiFe}(T)$ experimental data to Eq. (3), exhibiting a good agreement with the model in the entire T range. In the case of Ni NWs only the high-temperature data is close to the conditions of dominating K_{sh}, while the existence of a significative $MR^{\parallel}$ component at low T clearly indicates the presence of a reorientation of the NWs magnetization away from the long axis direction.

IV. DISCUSSION

A. Spin reorientation process

The $M(T)$ and MR(T) measurements allow us to determine the temperature dependence of the angle between M and the NW longitudinal direction [θ_M and θ_{MR}, respectively; Fig. 6(a)]. For the former, one uses $M = M_s^0 \cos(\theta)$, while for the latter the sum of the parallel and transverse resistance components has to be taken into account, i.e., $R(\theta) = R_{\perp} + (R_{\parallel} - R_{\perp})\cos^2(\theta)$.

A similar θ_M and θ_{MR} behavior is visible, although slight discrepancies appear at high temperatures (>150 K). This can be attributed to the distinct nature of the experimental methods employed. In fact, while $M(T)$ measurements provide the macroscopic state of the magnetization of the sample (long-range order), MR locally probes the degree of alignment between spins within the electron mean-free-path distance (short-range order). Nevertheless, a consistent increase of

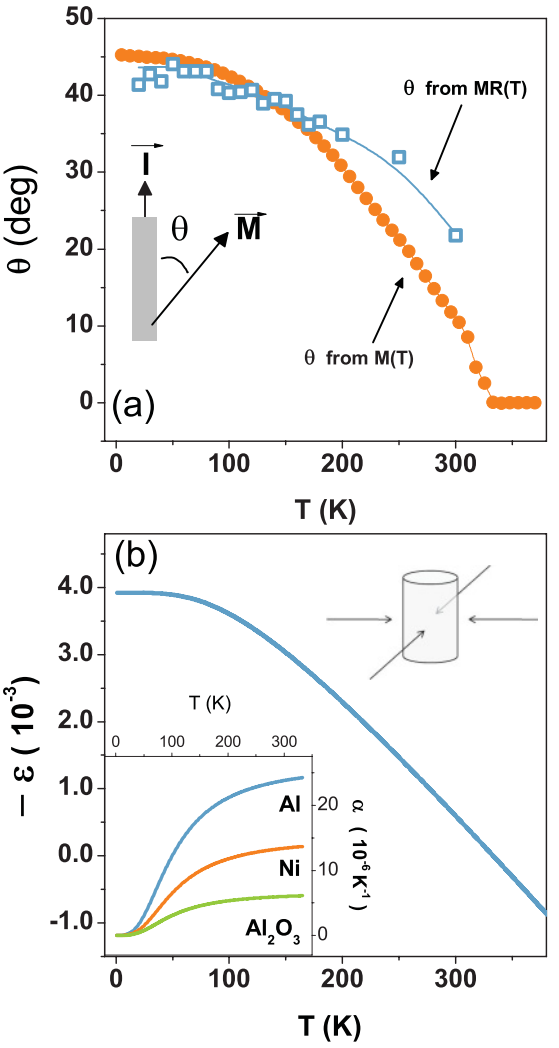

FIG. 6. (Color online) (a) $\theta(T)$ calculated from $M(T)$ [Fig. 3(b)] and MR(T) [Figs. 5(b) and 5(c)] measurements; the lines are a guide to the eye. (b) $\varepsilon(T)$ obtained from Eq. (4); the inset shows the temperature dependence of α_{Ni}, α_{Al}, and $\alpha_{Al_2O_3}$ calculated using the Debye model; notice the label $-\varepsilon$ in (b).

$\theta_{M,\mathrm{MR}}$ with decreasing T is present, reaching $\sim 43^\circ$ at low temperatures.

Noticeably, the magnetization of the NWs should follow Eq. (1) down to the deposition temperature (T_{dep}; $\sim$303 K). However, one observes that a significant misalignment already exists at 300 K, and that $M(T)$ starts to deviate from Eq. (1) at a higher temperature ($\sim$330 K). To explain this fact, one notes that a local temperature rise at the alumina-electrolyte interface during the formation of AAO has been reported.[37] The authors observed a temperature increase between 27 and 35 K for current densities $\sim$80–200 mA/cm^2, as a consequence of Joule heating dissipation in the insulator alumina barrier layer. In analogy, during the electrodeposition process, power dissipation is also expected at the bottom of the nanopores, leading to a localized temperature enhancement. Consequently, an effective (local) deposition temperature $\sim$20–40 K higher than the electrolyte bath and heating plate can be present during NW growth.

B. Contribution from the magnetoelastic anisotropy

A decrease in the MR value with decreasing T was also reported for a single-crystalline freestanding 30-nm Ni NW, and attributed to the temperature dependence of the magnetocrystalline anisotropy (K_{mc}).[21] Indeed, a spontaneous M reorientation from $\langle 111\rangle$ to $\langle 110\rangle$ crystallographic directions is present in bulk Ni with decreasing temperature.[38] Nevertheless, in polycrystalline and high-aspect-ratio NWs, K_{sh} is significantly large, and is therefore expected to dominate over K_{mc}. In fact, one has $K_{\mathrm{sh}}(300\ \mathrm{K}) = 7.2 \times 10^5$ ergs/cm^3 and $K_{\mathrm{sh}}(4.2\ \mathrm{K}) = 8.1 \times 10^5$ ergs/cm^3, while the bulk magnetocrystalline anisotropy constants of Ni are $K_1 = -4.5 \times 10^5$ ergs/cm^3 and $K_2 = -0.12 \times 10^5$ ergs/cm^3 at 300 K and $K_1 = -0.23 \times 10^5$ ergs/cm^3 and $K_2 = 0.3 \times 10^5$ ergs/cm^3 at 4.2 K.[39] Thus, in our NWs, the presence of a M reorientation should be mediated by another source of anisotropy besides K_{mc}. Previous works on the temperature-dependent magnetic properties [$M(H,T)$] of Ni NWs embedded in AAO reported a pronounced interplay between K_{sh} and the magnetoelastic anisotropy (K_{me}).[11–13] Upon cooling, the NWs become subject to a lateral compressive stress, a consequence of the large mismatch between the thermal expansion coefficients (α) of Al, AAO, and Ni.[10,12] Contrary to other materials (such as Fe, NiFe, and FeCo) where the positive (or null) magnetostriction constant (λ) reinforces K_{sh}, in Ni the (large) negative λ originates a significant magnetoelastic contribution. The result is a weaker effective anisotropy along the NW longitudinal axis that leads to a reorientation of the magnetization easy axis toward the transverse direction.[10–13,40]

Several authors considered as a first approximation a temperature-independent α.[10,12,13] However, and within the framework of the Debye model, $\alpha(T)$ is proportional to the specific heat capacity.[41] The inset of Fig. 6(b) shows $\alpha(T)$ for Ni, Al, and Al_2O_3 and, although, for $T > 200$ K, $\alpha(T)$ exhibits a fairly linear trend, a tendency toward a constant value is seen as we lower the temperature. The upper limit of the temperature-dependent strain [$\varepsilon(T)$] exercised by the Al on the Ni NWs is then given by the mismatch between α_{Al} and $\alpha_{\mathrm{Al_2O_3}}$, and can be calculated by[12,13,42]

$$\varepsilon(T) = \int_{T_{\mathrm{dep}}}^{T} [\alpha_{\mathrm{Al_2O_3}}(T) - \alpha_{\mathrm{Al}}(T)]dT. \tag{4}$$

Figure 6(b) displays $\varepsilon(T)$ imposed on the NWs by the Al/AAO, considering an effective T_{dep} of 330 K [i.e., $\varepsilon(330\ \mathrm{K}) = 0$] as inferred from θ_M. Remarkably, $\varepsilon(T)$ closely resembles the $\theta_{M,\mathrm{MR}}(T)$ curves obtained from the experimental measurements [Fig. 6(a)], reinforcing the crucial role of K_{me} in the observed reorientation of the magnetization. Notice particularly the saturation of both $\varepsilon(T)$ and $\theta_{M,\mathrm{MR}}(T)$ below $\sim$100 K.

Considering that the NWs are subjected to an in-plane biaxial strain,[43] the axial stress (σ_{ax}) is then obtained from

$$\sigma_{\mathrm{ax}} = \frac{\varepsilon(T)}{1 - \nu_{\mathrm{Ni}}} E_{\mathrm{Ni}},$$

with a Poisson coefficient of $\nu_{\mathrm{Ni}} = 0.31$ and a Young modulus of $E_{\mathrm{Ni}} = 230$ GPa.[12] For 4 K, one estimates $\sigma_{\mathrm{ax}} \simeq -1.3$ GPa ($\sigma_{\mathrm{ax}} < 0$ for compression); such a lateral compression, particularly in Ni, will favor an alignment of the magnetization along the contraction axis, i.e., transverse to the longitudinal NW direction.[38] Finally, for $\langle 110\rangle$ textured NWs, the temperature-dependent K_{me} term is calculated using $K_{\mathrm{me}}(T) = -\frac{3}{2}\lambda_{[110]}\sigma_{\mathrm{ax}}$, where $\lambda_{[110]}$ is the bulk saturation magnetostriction constant along $\langle 110\rangle$ ($\lambda_{[110]} = -30.1 \times 10^{-6}$).[44] We therefore obtain $K_{\mathrm{me}} \simeq 5.3 \times 10^5$ ergs/cm^3 (at 4.2 K), which is comparable to the K_{sh} value ($\sim 8.1 \times 10^5$ ergs/cm^3). This competition between K_{sh} and K_{me} qualitatively explains the reorientation of the magnetization easy axis.

C. Phenomenological energy model

To further clarify the nature of the observed M reorientation and in analogy to the in-plane to out-of-plane SRTs observed in ultrathin magnetic films,[15] we resort to a simple magnetic anisotropy energy model. To allow the presence of a monotonic rotation of the magnetization, one must take into consideration higher-order terms in the total energy of the system [$E(T,\theta)$].[14] A fourth-order expansion of $E(T,\theta)$ enables the existence of stable θ values between 0° and 90°, thus portraying the continuous nature of our temperature-driven SRT. The energy of the system is then given by (neglecting in-plane variations)

$$E(T,\theta) = K_2^{\mathrm{eff}}(T)\sin^2(\theta) + K_4^{\mathrm{eff}}(T)\sin^4(\theta). \tag{5}$$

In the above equation, the second-order effective anisotropy constant (K_2^{eff}) comprehends all the (second-order) magnetostatic terms, namely, shape and macroscopic demagnetizing anisotropies (K_{sh} and K_{md}, respectively), and the magnetoelastic anisotropy (K_{me}). K_{md} represents the anisotropy originating from the macroscopic demagnetizing field of the whole sample given by $K_{\mathrm{md}} = 4\pi M_s P$, where P is the sample porosity (usually $\sim$10% for a completely filled AAO).[6] For a cubic system, K_{mc} should appear only on fourth-order terms [$K_4^{\mathrm{eff}}(T)$] in addition to higher-order magnetoelastic terms and other possible sources of anisotropy.[45] For a continuous transition to occur [such as the one seen in Fig. 6(a)], this model requires $K_2^{\mathrm{eff}}(T) < 0$ and $K_4^{\mathrm{eff}}(T) > 0$ during the SRT.

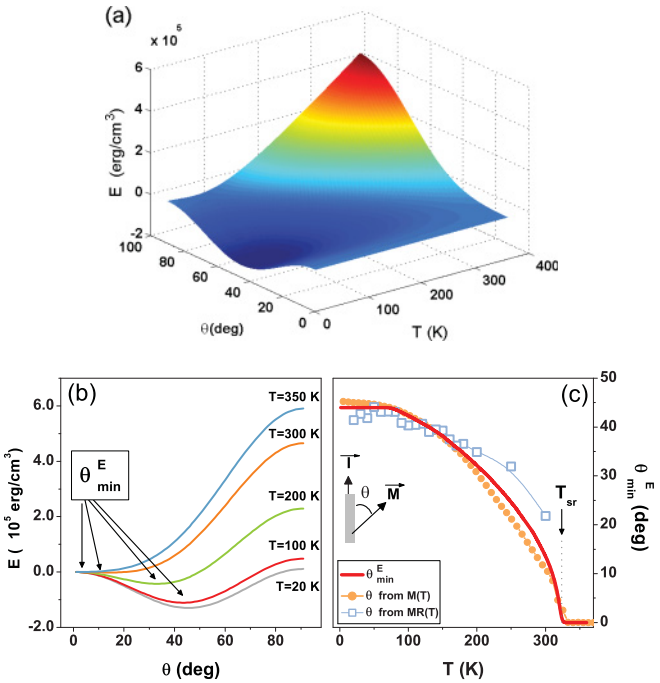

FIG. 7. (Color online) (a) Energy map for the Ni NWs system obtained from Eq. (5). (b) $E(\theta)$ curves for selected temperatures obtained from (a) and stressing the presence of a minimum angle at lower temperatures. (c) Comparison between $\theta^{E}_{\min}$ obtained from $E(T,\theta)$ minimization to the experimental $\theta_{M,\mathrm{MR}}$.

Within this framework, the decrease of $H_c^{\parallel}$ with T [see the inset of Fig. 3(b)] also supports $K_2^{\mathrm{eff}} < 0$; the latter leads to the weakly defined M easy axis along the NWs' long direction, which in turn translates into lower H_c values. Moreover, a crossover between $H_c^{\parallel}$ and $H_c^{\perp}$ is visible below ~150 K, from whereon small differences are observed between both H_c values. Such a characteristic is in close agreement with the saturation feature observed in $\theta(T)$ and $\varepsilon(T)$ [Fig. 6(c)].

Figure 7(a) displays the $E(T,\theta)$ color map for our Ni NW system, calculated using the already computed anisotropies, considering a K_{sh} value corrected for multidomain NWs (see below). A continuous variation with T of the energy minimum is visible, with an absolute minimum ~43° at low temperatures [<50 K; Fig. 7(b)]. The T-dependent angle (between M and the NW long axis) corresponding to the minimum of $E(T,\theta)[\theta^{E}_{\min}]$ is shown in Fig. 7(c). Notice that $\theta^{E}_{\min}(T)$, giving the stable canted magnetization state, follows the same trend as the experimentally obtained $\theta_{M,\mathrm{MR}}(T)$, mainly retaining the shape of $\varepsilon(T)$.

The best correlation of $\theta^{E}_{\min}$ with our experimental results was obtained for a shape anisotropy that is smaller (~60%–75%) than theoretically expected. This is expected, as the presence of local anisotropies arising from defects and finite dimensions lead to a decrease of the total anisotropy in NW systems, resulting in a multidomain structured NWs,[46–48] lower H_c values, and localized magnetization reversal.[8,49,50] Moreover, considering that such an accentuated K_{sh} decrease reflects the decrease in the demagnetizing factor ($N = 1/2$ for infinite long NWs), one obtains an effective NW monodomain length of ~47 nm. Such a value is in good accordance with theoretical results which consider the NWs as a magnetostatically coupled chain of ellipsoids with a monodomain size of ~20–30 nm.[48,51]

V. CONCLUSIONS

We presented a thorough study of the $M(T)$ and MR(T) behaviors in a temperature range between 5 and 370 K, for Ni and NiFe NWs with a diameter of ~35 nm and ~2 μm in length. The NiFe samples revealed the usual magnetic and transport behavior with temperature, consistent with dominant shape anisotropy. In contrast, we established a continuous rotation of the magnetization for Ni NWs from both $M(T)$ and MR(T) measurements. Due to the polycrystalline nature of our NWs, the origin of such anomalous phenomena required an additional source of anisotropy besides K_{mc}. The presence of a strong magnetoelastic contribution (perpendicular to the NW) was suggested, a consequence of the large mismatch between thermal expansion coefficients. Moreover, the continuous spin reorientation transition is successfully described using a fourth-order expansion of the energy of the system. The modeled angle between the magnetization and the NW axis showed a remarkable agreement with the experimental results, suggesting at the same time the presence of multidomain NWs with an average domain size of ~47 nm.

ACKNOWLEDGMENTS

Work supported in part by project FEDER/POCTI/n2-155/94 and PTDC/CTM/NAN/115125/2009. D.C.L., C.T.S., and A.M.P. are thankful for FCT Grants (No. SFRH/BPD/72359/2010, No. SFRH/BD/38290/2007, and No. SFRH/BPD/63150/2009). J.V. acknowledges funding through FSE/POPH. J.P.A. also thanks Fundação Gulbenkian for its financial support within the "Programa Gulbenkian de Estímulo a Investigação Científica."

*dleitao@fc.up.pt; now at INESC-MN and IN-Institute of Nanoscience and Nanotechnology, Rua Alves Redol 9, 1000-029 Lisboa, Portugal.

[1]W. Wernsdorfer, B. Doudin, D. Mailly, K. Hasselbach, A. Benoit, J. Meier, J. P. Ansermet, and B. Barbara, Phys. Rev. Lett. **77**, 1873 (1996).

[2]F. Elhoussine, S. Matefi-Tempfli, A. Encinas, and L. Piraux, Appl. Phys. Lett. **81**, 1681 (2002).

[3]D. Neumaier, A. Vogl, J. Eroms, and D. Weiss, Phys. Rev. B **78**, 174424 (2008).

[4]M. Vazquez, K. Pirota, M. Hernandez-Velez, V. M. Prida, D. Navas, R. Sanz, F. Batallan, and J. Velazquez, J. Appl. Phys. **95**, 6642 (2004).

[5]J. Escrig, R. Lavin, J. L. Palma, J. C. Denardin, D. Altbir, A. Cortes, and H. Gomez, Nanotechnology **19**, 075713 (2008).

[6]K. Nielsch, R. B. Wehrspohn, J. Barthel, J. Kirschner, U. Gosele, S. F. Fischer, and H. Kronmuller, Appl. Phys. Lett. **79**, 1360 (2001).
[7]L.-P. Carignan, C. Lacroix, A. Ouimet, M. Ciureanu, A. Yelon, and D. Menard, J. Appl. Phys. **102**, 023905 (2007).
[8]D. C. Leitao, C. T. Sousa, J. Ventura, K. R. Pirota, M. Vazquez, J. B. Sousa, and J. P. Araujo, J. Magn. Magn. Mater. **322**, 1319 (2010).
[9]H. Zeng, S. Michalski, R. D. Kirby, D. J. Sellmyer, L. Menon, and S. Bandyopadhyay, J. Phys. Condens. Matter. **14**, 715 (2002).
[10]S. Pignard, G. Goglio, A. Radulescu, L. Piraux, S. Dubois, A. Declemy, and J. L. Duvail, J. Appl. Phys. **87**, 824 (2000).
[11]J. Sanchez-Barriga, M. Lucas, F. Radu, E. Martin, M. Multigner, P. Marin, A. Hernando, and G. Rivero, Phys. Rev. B **80**, 184424 (2009).
[12]A. Kumar, S. Fahler, H. Schlorb, K. Leistner, and L. Schultz, Phys. Rev. B **73**, 064421 (2006).
[13]D. Navas, K. R. Pirota, P. M. Zelis, D. Velazquez, C. A. Ross, and M. Vazquez, J. Appl. Phys. **103**, 07D523 (2008).
[14]M. Farle, B. Mirwald-Schulz, A. N. Anisimov, W. Platow, and K. Baberschke, Phys. Rev. B **55**, 3708 (1997), and references therein.
[15]B. Schulz and K. Baberschke, Phys. Rev. B **50**, 13467 (1994), and references therein.
[16]I. Yamamoto, T. Nakagawa, Y. Takagi, and T. Yokoyama, Phys. Rev. B **81**, 214442 (2010).
[17]Q. Zhan, Z. Chen, D. Xue, F. Li, H. Kunkel, X. Zhou, R. Roshko, and G. Williams, Phys. Rev. B **66**, 134436 (2002).
[18]H. Zeng, R. Skomski, L. Menon, Y. Liu, S. Bandyopadhyay, and D. J. Sellmyer, Phys. Rev. B **65**, 134426 (2002).
[19]M. V. Kamalakar, A. K. Raychaudhuri, X. Wei, J. Teng, and P. D. Prewett, Appl. Phys. Lett. **95**, 013112 (2009).
[20]M. V. Kamalakar and A. K. Raychaudhuri, Phys. Rev. B **79**, 205417 (2009).
[21]Y. Rheem, B. Y. Yoo, W. P. Beyermann, and N. V. Myung, Nanotechnology **18**, 015202 (2007).
[22]Y. Rheem, B. Y. Yoo, B. K. Koo, W. P. Beyermann, and N. V. Myung, J. Phys. D **40**, 7267 (2007).
[23]H. Masuda and K. Fukuda, Science **268**, 1466 (1995).
[24]D. C. Leitao, A. Apolinario, C. T. Sousa, J. Ventura, J. B. Sousa, M. Vazquez, and J. P. Araujo, J. Phys. Chem. C **115**, 8567 (2011).
[25]K. Nielsch, J. Choi, K. Schwirn, R. B. Wehrspohn, and U. Gosele, Nano Lett. **2**, 677 (2002).
[26]K. Nielsch, F. Muller, A. P. Li, and U. Gosele, Adv. Mater. (Weinheim, Ger.) **12**, 582 (2000).
[27]C. T. Sousa, D. C. Leitao, M. P. Proenca, A. Apolinario, J. G. Correia, J. Ventura, and J. P. Araujo, Nanotechnology **22**, 315602 (2011).
[28]M. Schlesinger and M. Paunovic, *Modern Electroplating* (Wiley, New Jersey, 2000).
[29]F. Maurer, J. Brotz, S. Karim, M. Eugenia, T. Molares, C. Trautmann, and H. Fuess, Nanotechnology **18**, 135709 (2007).
[30]C. A. F. Vaz, J. A. C. Bland, and G. Lauhoff, Rep. Prog. Phys. **71**, 056501 (2008).
[31]D. Zhang, K. J. Klabunde, C. M. Sorensen, and G. C. Hadjipanayis, Phys. Rev. B **58**, 14167 (1998).
[32]M. Zheng, L. Menon, H. Zeng, Y. Liu, S. Bandyopadhyay, R. D. Kirby, and D. J. Sellmyer, Phys. Rev. B **62**, 12282 (2000).
[33]A. M. Pereira, J. B. Sousa, J. P. Araujo, C. Magen, P. A. Algarabel, L. Morellon, C. Marquina, and M. R. Ibarra, Phys. Rev. B **77**, 134404 (2008).
[34]D. C. Leitao, C. T. Sousa, J. Ventura, J. S. Amaral, F. Carpinteiro, K. R. Pirota, M. Vazquez, J. B. Sousa, and J. P. Araujo, J. Non-Cryst. Solids **354**, 5241 (2008).
[35]No discontinuous jumps in the $MR^{\perp,\parallel}$ curves are observed, a consequence of measuring several NWs in parallel. Also, for a parallel array of N equivalent NWs, the MR ratio is given by $\frac{1}{N}\sum_N[\frac{\Delta R_{NW}}{R_{NW}}] \simeq MR_{NW}$, i.e., nearly independent of the number of NWs.
[36]J. E. Wegrowe, D. Kelly, A. Franck, S. E. Gilbert, and J. P. Ansermet, Phys. Rev. Lett. **82**, 3681 (1999).
[37]I. De Graeve, H. Terryn, and G. E. Thompson, J. Appl. Electrochem. **32**, 73 (2002).
[38]R. M. Bozorth, *Ferromagnetism* (IEEE, New York, 1951).
[39]M. Hwang, M. Shima, C. A. Ross, C. Seberino, and H. N. Bertram, J. Appl. Phys. **92**, 1018 (2002).
[40]M. Ciria, F. J. Castaño, J. L. Diez-Ferrer, J. I. Arnaudas, B. G. Ng, R. C. O'Handley, and C. A. Ross, Phys. Rev. B **80**, 094417 (2009).
[41]C. Kittel, *Introduction to Solid State Physics*, 7th ed. (Wiley, New York, 1996).
[42]S. Kato, H. Kitazawa, and G. Kido, J. Magn. Magn. Mater. **272–276**, 1666 (2004).
[43]D. Navas, C. Nam, D. Velazquez, and C. A. Ross, Phys. Rev. B **81**, 224439 (2010).
[44]S. Chikazumi, *Physics of Magnetism* (Wiley, New York, 1959).
[45]M. Jamet, W. Wernsdorfer, C. Thirion, D. Mailly, V. Dupuis, P. Melinon, and A. Perez, Phys. Rev. Lett. **86**, 4676 (2001).
[46]Y. Henry, A. Iovan, J. M. George, and L. Piraux, Phys. Rev. B **66**, 184430 (2002).
[47]R. A. Guirado Lopez, J. M. Montejano-Carrizalez, and J. L. Moran-Lopez, Phys. Rev. B **77**, 134431 (2008).
[48]X. Lu, S. Ge, L. Jiang, and X. Wang, J. Appl. Phys. **97**, 084304 (2005).
[49]P. M. Paulus, F. Luis, M. Kroll, G. Schmid, and L. J. de Jongh, J. Magn. Magn. Mater. **224**, 180 (2001).
[50]H. B. Braun, Phys. Rev. Lett. **71**, 3557 (1993).
[51]F. Tian, J. Chen, J. Zhu, and D. Wei, J. Appl. Phys. **103**, 013901 (2008).
[52]American mineralogist crystal structure database, [http://rruff.geo.arizona.edu/AMS/amcsd.php].